Appl Magn Reson (2016) 47:223–235
DOI 10.1007/s00723-015-0741-9

Applied
Magnetic Resonance

Probing Flocculant-Induced Asphaltene Precipitation via NMR Imaging: from Model Toluene-Asphaltene Systems to Natural Crude Oils

E. V. Morozov[1,2,3] · O. N. Martyanov[3,4]

Received: 14 September 2015 / Revised: 18 October 2015 / Published online: 18 November 2015

Abstract An nuclear magnetic resonance (NMR) imaging approach for studying flocculant-induced asphaltene precipitation processes is introduced in this report. Unlike commonly accepted techniques, which primarily measure aggregation processes on the submicron scale (the level of asphaltene molecules and their aggregates), NMR imaging demonstrates the capability to obtain new useful information about bulk system behavior on the macro scale. To reveal the capabilities of the method, the model toluene-asphaltene system and two samples of natural crude oils with different chemical composition and physical properties (such as asphaltene content and density) were employed for experiments. The process of colloidal suspension formation and two different patterns of its evolution were observed depending on both the asphaltene content and the flocculant concentration. In the first pattern, the flocculant-induced precipitation leads to the slow uniform compacting of the suspension and descent of the sedimentation front, whereas the second pattern is characterized by sediment accumulation and the upwards drift of the front. It was found that the behavior of the precipitated asphaltenes in the model system correlates well with those observed in natural crude oils. The results achieved in this work are in agreement with the data obtained previously via other techniques. Thus, NMR imaging proved to be an efficient method for probing flocculant-induced precipitation in crude oils.

✉ E. V. Morozov
morozov_if@mail.ru

[1] Institute of Chemistry and Chemical Technology, Siberian Branch of the Russian Academy of Sciences, Akademgorodok 50/24, Krasnoyarsk 660036, Russia

[2] Kirensky Institute of Physics, Siberian Branch of the Russian Academy of Sciences, Akademgorodok 50/38, Krasnoyarsk 660036, Russia

[3] Boreskov Institute of Catalysis, Siberian Branch of the Russian Academy of Sciences, Pr. Ak. Lavrentieva 5, Novosibirsk 630090, Russia

[4] Novosibirsk State University, Pirogova st. 2, Novosibirsk 630090, Russia

1 Introduction

Crude oil production and processing is a challenging task for the petroleum industry due to the exorbitant expenses caused by the necessity of refining the pipelines, internal surface of the reservoirs, catalysts in the reactors from deposits. In spite of the thousands of components present in crude oil [1], the greatest contributors to deposit formation are asphaltenes [2, 3]. They are typically defined as the non-volatile fraction of crude oils that are insoluble in *n*-alkanes [4]. This definition captures the heaviest fraction of crude oil, which is composed of a broad distribution of molecules that have a strong tendency for destabilization and phase separation. There are still some discussions regarding the structure of asphaltene molecules at the moment, but in general, they are considered to be formed by a system of polyaromatic layers with different functional groups and alkyl chains [5]. The theories regarding the asphaltene states in crude oil are also controversial; nevertheless, it is generally accepted that they exhibit colloidal behavior in crude oil, resulting in association and aggregation processes, followed by precipitation under external factors, such as temperature, pressure, and chemical composition changes [6].

Aggregation of asphaltenes followed by precipitation determines the behavior of crude oil during processing, and consequently, much effort has been devoted to studying these processes from molecular to industrial scales. To achieve this aim, a number of methods were intensively employed: Fourier transform infrared (FTIR), nuclear magnetic resonance (NMR) and electron spin resonance (ESR) spectroscopy [7–12], small-angle neutron and X-ray scattering [13, 14], X-ray diffraction [15], optical fluorescence [16], dynamic light scattering [17, 18], ultracentrifugation [19], viscometry and calorimetry [20–22], optical and electron microscopy [23–25] etc. Most of these methods work well on the molecular and nanoaggregate scale, giving valuable information about the asphaltene structure, their interactions, and the morphology of the aggregates. At the same time, some approaches only provide information about the rheological properties, mass of deposits or precipitation point. It would be beneficial to use a method that can determine the bulk properties in situ and establish their interrelation with the phase behavior of oil.

A literature analysis revealed that very few studies used NMR imaging (MRI) to study asphaltene. At the same time, this method has been successfully applied to many areas of research [26, 27] and has been found to be an advanced technique for the non-destructive visualization of the various processes occurring in optically opaque systems. The main problem that restricts NMR imaging applications to the study of asphaltene precipitation is the low spatial resolution of the method (generally the best resolution is ~ 50 μm in a slice plane for the most commonly used equipment). The size of the particles that form aggregates in crude oil systems is much smaller than the resolution of NMR imaging [28]. For this reason, the NMR images of the colloids usually appear to be homogeneous, even for systems consisting of a number of different constituents. However, some processes occurring in such colloidal systems may result in the formation of spatially separated domains with a diverse composition and/or structure accompanied by interfaces. For

instance, the sedimentation process in a suspension may lead to deposit formation at the bottom of the container with a clear interface between the two parts. This occurs if the size of the different domains sufficiently exceeds the resolution of the method. In this case, they can be visualized if the differences in the relaxation times or other NMR parameters, such as the diffusion coefficient, density of nuclei, and so on, that contribute to the image contrast are provided. As a result, the initially homogeneous system, in terms of resolution, can be visualized as the spatially separated domains with the further probing of their interfaces' dynamics during any process that can occur in the system. By using this approach, it is possible to apply NMR imaging to monitor asphaltene precipitation.

In this study, the NMR imaging approach was introduced for probing flocculant-induced asphaltene precipitation. To demonstrate its feasibility, the method was tested for two samples of natural crude oils with diverse properties and chemical compositions. It was previously found that NMR imaging was able to visualize the interfacial flocculation processes in aged asphalts–isooctane–toluene blends [29]. Unfortunately, due to the complicated nature of the oxidized asphalts used, the investigation of the influence of asphaltene and the flocculant concentration on the mechanisms of precipitation was beyond the scope of that study. To avoid such problems and reliably interpret the data obtained, the model toluene–asphaltenes system was studied first. The images observed were brought into correlation with those obtained for natural crude oils.

2 Experimental Section

2.1 Samples Preparation

Two types of samples were prepared for the experiments. Asphaltene solutions in toluene were the first type and used as model samples. Asphaltenes were extracted from Tatarstan heavy crude oil following the method of ASTM D6560-00 (Standard Test Method for Determination of Asphaltenes (Heptane Insolubles) in Crude Petroleum and Petroleum Products [30]) substituting heptane and toluene as solvents for hexane and benzene, respectively. All of the solvents used were reagent or higher grade.

The second type of sample was natural crude oils with a different chemical composition and physical properties similar to those described previously [31]. Crude oils with different characteristics were deliberately chosen to test the divergent conditions of the asphaltene aggregation processes. So, oil 1 is characterized by a high asphaltene content and high density (6 wt% and 932 kg/m^3, respectively), whereas oil 2 contains low amounts of asphaltenes and has sufficiently lower density (0.4 wt% and 823 kg/m^3, respectively). The concentration of asphaltenes in the model samples was adjusted to be 6 wt%, which allowed the results to be compared with those obtained for the oil 1 crude sample. For the initiation of the aggregation processes in both types of samples, *n*-heptane was used as a flocculant.

Liquid samples were poured in a flat-bottom glass tube (7-mm inner diameter) at room temperature followed by careful stirring with *n*-heptane at given ratios. The

overall volume of the specimen loaded into the tube was approximately 1 mL. After blending, the tube with the sample was inserted into the MRI probe, and the NMR image acquisition process was started immediately. A temperature of 25 ± 2 °C was maintained during the measurement.

2.2 Equipment and Methods

The imaging experiments were carried out using an NMR imaging installation based on a Bruker AVANCE DPX 200 console and superconducting magnet with an 89-mm diameter vertical bore, water-cooled and self-shielded Bruker gradient set (maximum gradient strength up to 292 mT/m); probe PH MINI 0.75, 38-mm internal diameter birdcage coil tuned and matched to ^{1}H nuclear resonance frequency of 200.13 MHz; and a console operated with Paravision 4.0 software.

The principles of the NMR imaging technique are well known and are not presented here (the basic information about how it works can be found in [26, 27, 32]). Slice selective 2D NMR images were acquired using the spin-echo-based pulse sequence supplied by the imager software: T_2-weighted images were acquired by the rapid acquisition with relaxation enhancement (RARE) technique; T_2 maps were plotted by the processing of the image sequences acquired by the multi slice multi echo (MSME) technique (using standard Image Sequence Analysis option supplied by software). Variation of proton density in the samples is expected to be too low to provide reliable contrast in proton density weighted images: concentration of the densest fraction of asphaltenes is only 6 wt% and this fraction still contains the protons. For comparison, pd-weighted images considered to be reliable in systems containing inorganic particles which able to form dense sediment [33].

The parameters of image acquisition were as follows: slice thickness of 1 mm; field of view (FOV) of 40 mm; and matrixes of 128 9 128 (T_2 maps) and 256 9 256 pixels (T_2-weighted images). The repetition time (TR) and echo time (TE) were adjusted over a wide range depending on the sample's T_1 and T_2 to provide the best contrast. The time of image acquisition (TA) resulted from the TR and TE parameters, and the number of scans was maintained as short as possible; the echo train for the RARE technique consisted of 128 equally spaced echoes, and the number of echoes for the MSME technique was 28. Spatial T_2 profiles were evaluated by plotting T_2 vs. the coordinate corresponding to the position of the pixel on the T_2 map (all of the profiles presented in this work are plotted along the vertical axis of the tube with the sample). Despite the multiexponential nature of spin–spin relaxation in complex organic mixtures, NMR imaging works with an effective T_2. This value comprises all contributions with their partial weights, and T_2-weighted images are sensitive to changes of the relaxation time itself and weight of corresponding components.

It is worth noting that NMR imaging method itself may influence on the systems investigated due to acoustic noise and vibrations during the image acquisition. Careful analysis, however, revealed no presence of such influence: variation of pulse sequence parameters TR and TE has caused different intensity of vibration, but system behavior was not affected at all. This issue also has been investigated

previously in more sensitive systems and it was found that the effect of vibrations on the studied systems is negligible [34].

3 Results and Discussion

3.1 Asphaltenes Precipitation from Toluene Solution

Initially, the toluene-asphaltene samples demonstrated a homogeneous distribution of the NMR signal/T_2 relaxation time in the images independent of the contrast scheme used for visualization. The images of the *n*-heptane/toluene–asphaltenes blend with a flocculant to initial specimen volume ratio of 2:1 displayed two diverse regions right after stirring. The effective spin–spin relaxation times differ dramatically for these regions, providing deep contrast, which is shown in Fig. 1. The sequence of the NMR images (Fig. 1) reflects the evolution of the blend with time. Due to the nature of the system consisting only of mobile molecules of *n*-heptane/toluene (with long T_2) and relatively immobile molecules of asphaltenes (with short T_2), the upper and lower regions visualized should be obviously attributed to the asphaltenes-depleted and asphaltenes-enriched parts, respectively. The relaxation time of asphaltene molecules, however, is likely too short to contribute to NMR signal; therefore, the apparent decreasing of T_2 in asphaltenes-enriched part is associated with reduction of the relaxation times of the small organic components (with the reduction progressing as the concentration of asphaltenes increasing in the lower part of the sample). It is difficult to state the precise mechanism leading to the shortening of the T_2: the relaxation time is affected by many factors such as density, magnetic susceptibility, diffusion coefficient, chemical composition and/or structure and many others, because these parameters can change the correlation time of fluctuating local magnetic field. Whatever the mechanism, increasing the asphaltenes concentration in the lower part of the system is detected by MRI. It is worth to note also that the relaxation times within every region appeared to be homogeneously distributed and that no additional domains inside each of them were found.

Different compositions of the split domains determine their evolution in different ways. The asphaltene-depleted region revealed the stability of T_2 along the whole process, which is apparently demonstrated by the T_2-profiles plotted along the

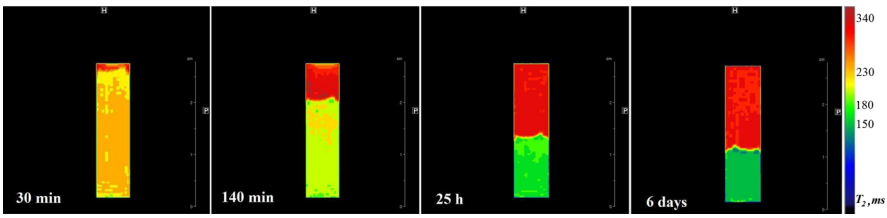

Fig. 1 Sequence of the T_2 maps of the *n*-heptane/toluene–asphaltenes blend during system evolution (flocculant to sample volume ratio of 2:1); the time after *stirring* is represented in every *image*

vertical axis during evolution of the blend (Fig. 2a). In contrast, the asphaltenes-enriched lower region shows a slow decrease of T_2 with time. Relaxation time reduction in this region may indicate that (a) partial weight of the fast relaxation component is growing up (that corresponds to the growth of asphaltenes concentration); (b) relaxation time itself in this part is decreasing (it means that the motion of small organic components is becoming more restricted). As seen, the interface between the regions described drifts downwards in a nonlinear manner (Fig. 3): in the beginning there is a very fast linear decreasing of normalized height which is followed by a slow nonlinear reaching of equilibrium state. Such behavior of the interface, which is accompanied by the T_2 decrease mentioned above, indicates that the asphaltenes-enriched region has to be considered as a suspension comprising the aggregates of asphaltenes. The action of gravity on the aggregated particles causes their settling, which in turns leads to the compaction of suspension followed by an increase of the mean density. Hydrodynamic interaction of settling particles causes also a well-known effect of interface self-sharpening [33, 34]: reduced T_2 value can be observed at the interface in T_2-profiles (Fig. 2). Nevertheless, the compaction of the suspension cannot be described as a simple sedimentation process: settling particles must form the sediment layer at the bottom,

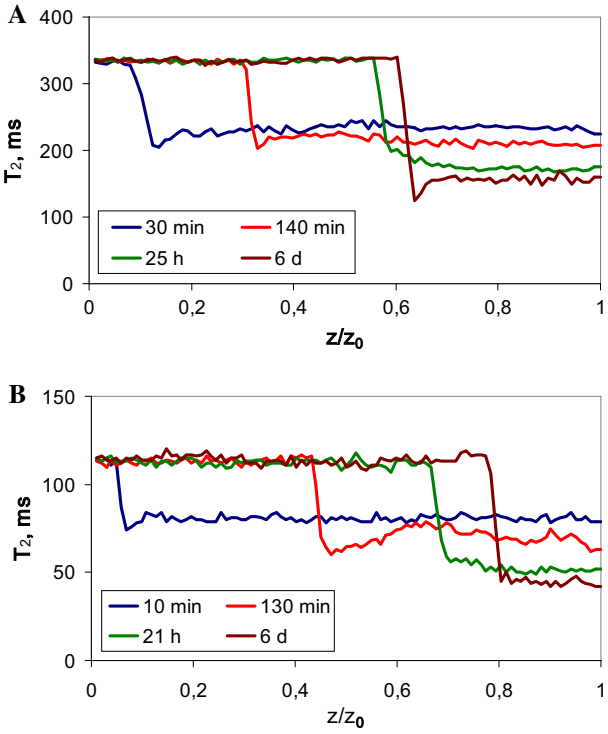

Fig. 2 Evolution of the T_2 profiles along the *vertical axis* of the tube with the *n*-heptane/toluene–asphaltenes blend (**a**) and *n*-heptane-oil 1 blend (**b**). The *zero point* corresponds to the *upper* level of the sample

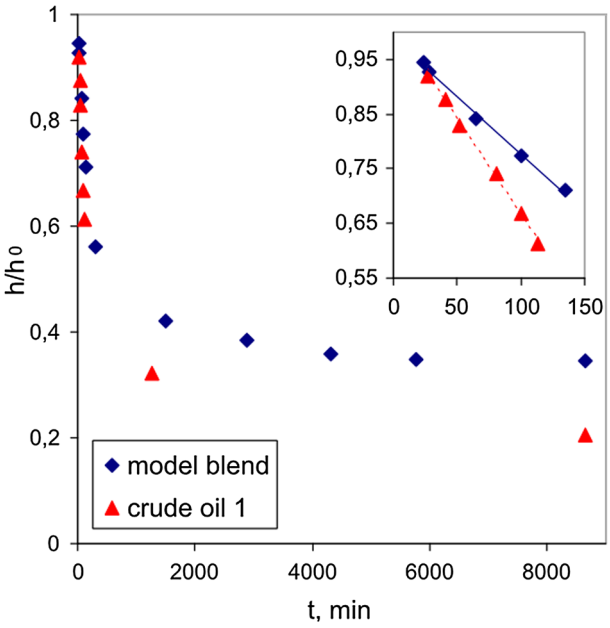

Fig. 3 Descending of the normalized height h/h_0 of interface with time for model blend and oil 1 sample

which is always accompanied by stratification [33]. However, neither sediment accumulation at the bottom nor stratification of the asphaltenes-enriched region was observed using various contrast-enhanced schemes and analysis of T_2-profiles.

The behavior of the blends was found to be dependent on the flocculant concentration. For blends with a sufficient excess of flocculant, the asphaltene precipitation appears in the same way as described above, regardless of the ratio 2:1 or 4:1, for example. In every case, the asphaltene-enriched region can be visualized clearly, which enables the measurement of its relaxation time and spatial dynamics. When the flocculant–sample ratio is 1:1 or less, NMR images demonstrate homogeneously distributed signal intensity/relaxation times over the blend during

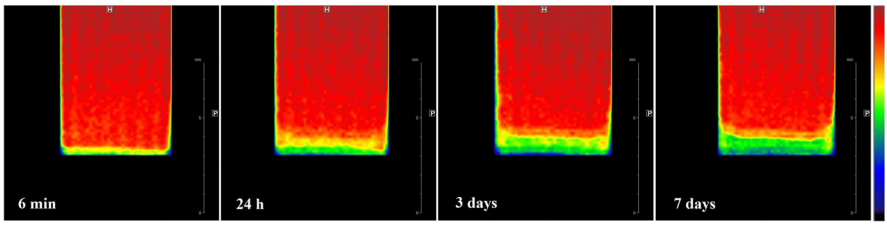

Fig. 4 Sequence of the T_2-weighted images of the *n*-heptane/toluene–asphaltenes blend during system evolution (flocculant to sample volume ratio is 1:1); the time after *stirring* is represented in every *image*. Parameters: TR = 20 s, TE = 347 ms, TA = 2 min 40 s. For convenience only the *bottom part* of the tube with the *blend* is presented

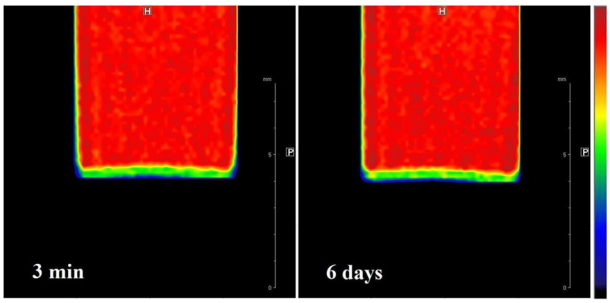

Fig. 5 T_2-weighted images of the *n*-heptane/toluene–asphaltenes blend (flocculant to sample volume ratio is 0.5:1); the time after *stirring* is represented in every *image*. Parameters: TR = 20 s, TE = 347 ms, TA = 2 min 40 s. The *bottom part* of the tube with the *blend* is presented

the first 12 h. Only after approximately 24 h does NMR imaging allow visualization of a new region near the bottom of the tube (Fig. 4, for convenience, the T_2-weighted images are presented instead of the T_2 maps due to their higher sensitivity and contrast). In contrast to the previous case, the interface between two regions appears to be smooth and drifts upward with time. The lower visualized region can be attributed to the sediment consisting of precipitated asphaltenes. The small size of the particles does not allow them to be visualized separately; slow settling under the action of gravity forms the sediment in a multilayer manner (at least two thin layers can be observed in Fig. 4), reflecting the particles size distribution. It should be concluded that flocculant-induced aggregation occurring in the blends results in the formation of suspensions followed by sedimentation via different mechanisms: excess flocculant turns the blend into a suspension prone to uniform compacting, otherwise the blend becomes a suspension with particles that grows and slowly settles, forming layers of sediment.

The NMR images of blends with a very low flocculant–sample ratio (0.5:1) demonstrate a homogeneous signal intensity distribution that is as long as the study period (Fig. 5, the thin layer near the bottom could not be caused by the precipitation of asphaltenes because the first image was taken right after stirring and all of the other images that were taken after demonstrate exactly the same picture). The asphaltenes could aggregate in this blend, but the particles formed did not settle down and no precipitation was observed via MRI.

3.2 Asphaltenes Precipitation from Natural Crude Oils

Model toluene–asphaltenes samples clearly indicate where the asphaltenes-enriched regions appeared during flocculant-induced precipitation. This became possible because of the large difference between the proton relaxation times for the heptane/toluene molecules and complex heteronuclear polyaromatic compounds (asphaltenes) [35, 36]. This more complicated behavior can be expected in crude oils that are mixtures of very different compounds.

NMR images of oils 1 and 2 before stirring with flocculant showed a homogeneous picture, but images of the *n*-heptane-oil 1 blend with different flocculant to oil ratios surprisingly demonstrated a similar pattern to that found in the model toluene–asphaltenes samples. In the case where there is an excess of the *n*-heptane in a blend, two regions immediately appear with very different magnitudes of relaxation times (Fig. 6, the flocculant to oil sample ratio is 2:1). It can be reasonably suggested that the lower region should also be attributed to an asphaltene-enriched suspension; it is well known that asphaltenes contain the heaviest molecules (with a very short relaxation time, T_2) and paramagnetic species (for example, vanadyl centers [12]) that, in total, provide a large difference in T_2 magnitudes between asphaltene-enriched and asphaltene-depleted parts of *n*-heptane-oil species. The relaxation dynamics of the lower region demonstrates the slow decrease of T_2, whereas the upper region keeps T_2 stable during the whole period of time (see the profiles in Fig. 2b). The dynamics of interface showed a very similar behavior to that observed for model blend (Fig. 3): fast linear decreasing of normalized height in the beginning is followed by a slower tail of sedimentation. Therefore, the very similar relaxation dynamics, slow uniform compaction and downward drift of the interface prove the similarity of the behavior of asphaltenes in the model system and real oil in the presence of flocculant excess.

Along with this similarity, NMR imaging appears to be able to reveal some of the differences between the behavior of the model sample-flocculant and the oil 1-flocculant blends. As seen in Figs. 2 and 6, the asphaltenes-enriched region is not as uniform as it was in the model blend. Moreover, the compaction process in the crude oil-flocculant blend eventually turns the suspension into a "clot" that keeps its shape (Fig. 5d, a thin layer of the mixture between the surface and walls can be observed). Additionally, the compaction degrees observed through the profiles shown in Fig. 2 were found to be sufficiently larger for the clot compared to the model system (approximately 0.8 in 6 days against 0.6 for the model sample at the same time). All of these differences arise from the complex composition of crude oil: it is well known that resin and aromatic molecules in natural oil actively interact with asphaltenes, forming micelles in suspension and strong gel-like structures after precipitation [37–39]. Inversely, the model sample contains only asphaltenes, and flocculant-induced precipitation may yield a relatively loose suspension composed of particles with a weak gel-like network.

When the flocculant–oil ratio approaches 1:1, the NMR images demonstrate slow accumulation of sediment on the bottom of tube (Fig. 7). However, in this case, the

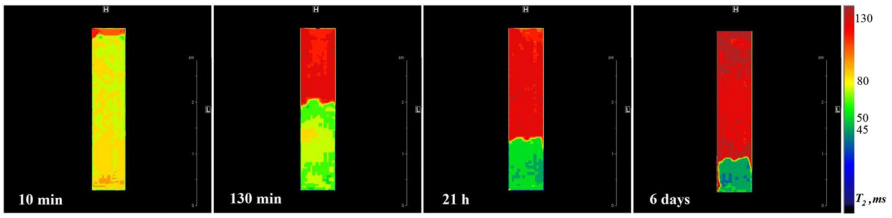

Fig. 6 Sequence of the T_2 maps of the *n*-heptane-oil 1 blend during system evolution (flocculant to sample volume ratio is 2:1); the time after *stirring* is represented in every *image*

sedimentation processes occur very fast compared to the model sample, and 2–5 h after stirring, the precipitated particles have already formed the sediment. The images acquired after this time demonstrate that accumulation turns into the slow compaction of sediment layer (Fig. 7, 7 h). Despite some differences, the pattern of asphaltene sedimentation in oil should be considered to be the same as for the model system. The further decrease of flocculant amount in the blend eventually leads to the increase in system stability; the images continue to be homogeneous for as long as they were studied (similar to that presented in Fig. 5).

As was described above, NMR imaging revealed that the flocculant-induced precipitation in the *n*-heptane/toluene–asphaltenes and *n*-heptane-oil 1 blends occurs according to the same patterns. However, images of the *n*-heptane-oil 2 blends, even at very high flocculant–sample ratios, only revealed sediment accumulation processes similar to those observed in the model sample and *n*-heptane-oil 1 blend with a 1:1 ratio (Fig. 8, images of different flocculant-oil 2 blends are shown). In every case, the upward drift of the interface was tracked and the sediment region was clearly visible through any contrast scheme used. The sole pattern of sedimentation in these blends definitely originates from the fact that oil 2 is light with a low asphaltene and resin content (amount of asphaltenes here is 15 times less than that in oil 1). This amount is insufficient for yielding suspensions that are prone to slow compaction; the precipitated particles could not be properly stabilized and settled, forming the observed layer of sediment. Thus, NMR imaging provides a visualization of the sediment layers up to an *n*-heptane-oil 2 ratio of 0.25:1, at which point, sedimentation processes no longer occurred. This method is therefore appropriate for probing sedimentation patterns in a wide range of flocculant to sample ratios as well as asphaltene contents.

The behavior of the blends studied in this work via NMR imaging correlates well with the data found previously by other methods. It is commonly accepted that flocculant-induced asphaltene precipitation is a complex process that involves an initial aggregation, growth of particles, formation of agglomerates with a wide size distribution, sedimentation and deposit formation [40]. Although the aggregation processes were studied comprehensively and the mechanisms of micelle formation and their thermodynamics now can be considered to be generally solved through experiments and computational modeling [5, 41–43], only a few works actually presented data that were obtained in situ concerning the evolution of the system's bulk during flocculant-induced asphaltene precipitation. For this reason, the

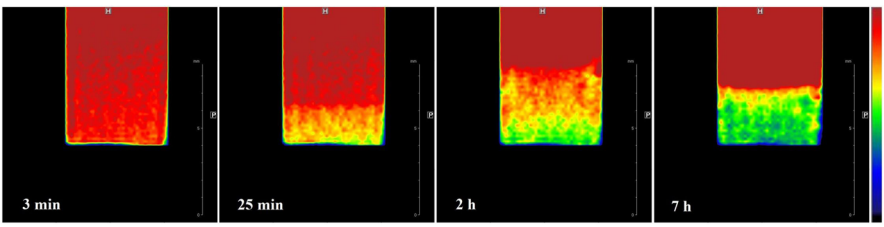

Fig. 7 Sequence of the T_2-weighted images of the *n*-heptane-oil 1 blend during system evolution (flocculant to sample ratio is 1.2:1); the time after *stirring* is represented. Parameters: TR = 8 s, TE = 231 ms, TA = 1 min 4 s. The *bottom part* of the tube with the *blend* is presented

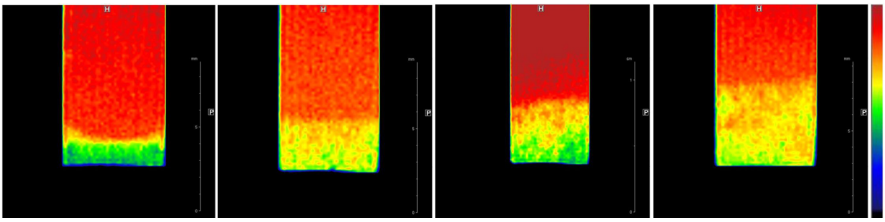

Fig. 8 T_2-weighted images of the *n*-heptane-oil 2 blends; the flocculant to sample ratios are 0.5:1 (**a**), 1:1 (**b**), 2:1 (**c**) and 5:1 (**d**). Parameters: TR = 20 s, TE = 341 ms, TA = 2 min 40 s. The *bottom part* of the tube with the *blend* is presented

different patterns of sedimentation observed through NMR imaging cannot be directly compared with the results obtained by other methods. Nevertheless, some of the findings are compatible. Thus, it was recently found that the increase of the asphaltene content in the systems with initial asphaltene concentrations above 1 wt% yielded a sufficient decrease of the rate of asphaltene aggregation due to the effects of mutual stabilization by different asphaltenes subfractions [44]. Indeed, the second pattern of sedimentation was found to be very fast compared to the first one: a noticeable layer of the sediment can be observed within several hours (or in 1 day for the model system), whereas the compacted deposit (clot) is completely formed in a few days. The second pattern was revealed in *n*-heptane-oil 2 blends where the asphaltene concentration is below 1 wt% (0.4 wt%, subsection 2.1). The fact that this pattern was also observed in the system with asphaltene concentrations that were much higher than 1 wt% can be explained by the presence of several types of asphaltene molecules containing different functional groups with heteroatoms. It was determined that a small amount of the flocculant in the blend is able to destabilize only the most unstable asphaltenes [45–47]. An excess of flocculant totally destabilizes all of the different types of asphaltenes present in the system, which in turns yields the first pattern of suspension behavior.

A different behavior of the sedimentation front (dynamics of the interface) was also observed in [18] through dynamic light scattering and bulk sedimentation experiments; depending on the amount of flocculant, the sedimentation front is observed (1) initially near the top of the sample and then drifts downwards in a nonlinear fashion to reach its equilibrium level or (2) initially near the bottom of the sample and then drifts upwards. This behavior is very similar to those that we found in the model toluene-asphaltene systems and crude oils via NMR imaging. Reproducibility of the behavior described and its agreement with data obtained previously by different techniques proves results to be relevant.

4 Conclusions

NMR imaging approach for probing the behavior of model toluene-asphaltene systems and crude oils with different properties and chemical compositions after the addition of flocculant was presented in this work. Results obtained demonstrate the

feasibility of this technique for visualization of asphaltene precipitation. NMR images show different patterns of precipitation that depend on both the flocculant and asphaltene concentrations in the blends. Thus, high flocculant to sample ratios turn blends with 6 wt% of asphaltenes into suspensions that are characterized by slow uniform compaction and a downward drift of the sedimentation front. Considerably lower flocculant concentration turns the same blends into a suspension characterized by sediment accumulation at the bottom and an upward drift of the sedimentation front. The model *n*-heptane/toluene–asphaltenes blend was used to identify the asphaltenes-enriched and asphaltenes-depleted domains observed in the NMR images. Adjusting the contrast in the images and using the T_2 maps enabled the proper visualization of the appropriate regions and the quantitative measurement of their dynamics. The results achieved in this work are consistent with the generally accepted model of asphaltenes precipitation and compatible with observations carried out by other methods. This approach appeared to be useful for the further investigation of the asphaltenes behavior in a mixture of natural oils, when one of them could become a flocculant for another. Practically, the NMR imaging approach could be applied in situ for precipitation onset determination and/or discriminating of sedimentation pattern. It has a special significance in the case, when micro (molecular) scale behavior of asphaltene demonstrates that aggregation processes in the system do occur, while they do not result in bulk deposit formation.

Acknowledgments This research was performed with the financial support of Russian Science Foundation (project no. 15-19-00119).

References

1. C.A. Hughey, R.P. Rodgers, A.G. Marshall, Anal. Chem. **74**(16), 4145 (2002)
2. J.G. Speight, *The Chemistry and Technology of Petroleum*, 4th edn. (CRC Press/Taylor & Francis, Boca Raton, 2007)
3. J.J. Adams, Energy Fuels **28**, 2831 (2014)
4. M.P. Hoepfner, V. Limsakoune, V. Chuenmeechao, T. Maqbool, H.S. Fogler, Energy Fuels **27**, 725 (2013)
5. J. Sjöbloma, S. Simon, Z. Xu, Adv. Colloid Interface Sci. **218**, 1 (2015)
6. E.B. Sirota, M.Y. Lin, Energy Fuels **21**, 2809 (2007)
7. I. Auflem, T. Havre, J. Sjöblom, Colloid Polym. Sci. **280**, 695 (2002)
8. R.R. Coelho, I. Hovell, E.L. Moreno, A.L. de Souza, K. Rajagopal, Pet. Sci. Technol. **25**, 41 (2007)
9. N.V. Lisitza, D.E. Freed, P.N. Sen, Y.-Q. Song, Energy Fuels **23**, 1189 (2009)
10. E.C. Oliveira, Á.C. Neto, V.L. Júnior, E.V.R. de Castro, S.M.C. de Menezes, Fuel **117**, 146 (2014)
11. M.I. Tagirzyanov, M.R. Yakubov, G.V. Romanov, J. Can. Pet. Technol. **46**, 9 (2007)
12. S.N. Trukhan, V.F. Yudanov, A.A. Gabrienko, V. Subramani, S.G. Kazarian, O.N. Martyanov, Energy Fuels **28**, 6315 (2014)
13. J.C. Ravey, G. Ducouret, D. Espinat, Fuel **67**, 1560 (1988)
14. F.V. Tuzikov, YuV Larichev, L.S. Borisova, I.V. Kozhevnikov, O.N. Martyanov, Pet. Chem. **51**(4), 281 (2011)
15. S.I. Andersen, J.O. Jensen, J.G. Speight, Energy Fuels **19**, 2371 (2005)
16. H. Groenzin, O.C. Mullins, Energy Fuels **14**, 677 (2000)
17. Y.G. Burya, I.K. Yudin, V.A. Dechabo, V.I. Kosov, M.A. Anisimov, Appl. Opt. **40**, 4028 (2001)
18. S.M. Hashmi, A. Firoozabadi, J. Phys. Chem. B **114**, 15780 (2010)
19. F. Mostowfi, K. Indo, O.C. Mullins, R. McFarlane, Energy Fuels **23**, 1194 (2008)
20. I.N. Evdokimov, DYu. Eliseev, NYu. Eliseev, J. Pet. Sci. Eng. **30**(3/4), 199 (2001)

21. S.I. Andersen, S.D. Christensen, Energy Fuels **14**, 38 (2000)
22. S.I. Andersen, K.S. Birdi, J. Colloid Interface Sci. **142**, 497 (1991)
23. G.W. Zajac, N.K. Sethi, J.T. Joseph, Scanning Microsc. **8**, 463 (1994)
24. S. Acevedo, P. Rodriguez, Energy Fuels **18**, 1757 (2004)
25. C.M. Seifried, J. Crawshaw, E.S. Boek, Energy Fuels **27**, 1865 (2013)
26. I.V. Koptyug, R.Z. Sagdeev, Russ. Chem. Rev. **71**(7), 593 (2002)
27. S. Stapf, S.-I. Han, *NMR Imaging in Chemical Engineering* (WILEY-VCH, Weinheim, 2006)
28. H.W. Yarranton, D.P. Ortiz, D.M. Barrera, E.N. Baydak, L. Barré, D. Frot, J. Eyssautier, H. Zeng, Z. Xu, G. Dechaine, M. Becerra, J.M. Shaw, A.M. McKenna, M.M. Mapolelo, C. Bohne, Z. Yang, J. Oake, Energy Fuels **27**, 5083 (2013)
29. F.P. Miknis, A.T. Pauli, L.C. Michon, D.A. Netzel, Fuel **77**, 399 (1998)
30. http://www.astm.org/Standards/D6560.html
31. L.S. Borisova, Oil Gas Geol. **1**, 76 (2009)
32. P. Callaghan, *Principles of Nuclear Magnetic Resonance Microscopic* (Clarendon Press, Oxford, 1993)
33. J. Acosta-Cabronero, L.D. Hall, AlChE J. **55**, 1426 (2009)
34. E.V. Morozov, O.V. Shabanova, O.V. Falaleev, Appl. Magn. Reson. **44**(5), 619 (2013)
35. I.N. Evdokimov, NYu. Eliseev, B.R. Akhmetov, Fuel **82**, 817 (2003)
36. J. Jestin, L. Barre, J. Dispersion Sci. Technol. **25**(3), 341 (2004)
37. M.A. Anisimov, Yu.M. Ganeeva, E.E. Gorodetskii, V.A. Deshabo, V.I. Kosov, V.N Kuryakov, D.I. Yudin, I.K. Yudin, Energy Fuels **28**, 6200 (2014)
38. J.I.S. Aguiar, C.R.E. Mansur, Fuel **140**, 462 (2015)
39. H.W. Yarranton, J. Dispersion Sci. Technol. **26**, 5 (2005)
40. J.S. Buckley, Energy Fuels **26**, 4086 (2012)
41. E. Forte, S.E. Taylor, Adv. Colloid Interface Sci. **217**, 1 (2015)
42. J.F. Jover, E.A. Müller, A.J. Haslam, A. Galindo, G. Jackson, H. Toulhoat, C. Nieto-Draghi, Energy Fuels **29**(2), 556 (2015)
43. P.-A. Artola, F.E. Pereira, C.S. Adjiman, A. Galindo, E.A. Müller, G. Jackson, A.J. Haslam, Fluid Phase Equilib. **306**(1), 129 (2011)
44. N. Haji-Akbari, P. Teeraphapkul, H.S. Fogler, Energy Fuels **28**, 909 (2014)
45. A.A. Gabrienko, V. Subramani, O.N. Martyanov, S.G. Kazarian, Adsorpt. Sci. Technol. **32**, 243 (2014)
46. A.A. Gabrienko, E.V. Morozov, V. Subramani, O.N. Martyanov, S.G. Kazarian, J. Phys. Chem. C **119**, 2646 (2015)
47. M. Sedghi, L. Goual, W. Welch, J. Kubelka, J. Phys. Chem. B **117**, 5765 (2013)